NeuroImage 198 (2019) 93–103

Contents lists available at ScienceDirect

NeuroImage

journal homepage: www.elsevier.com/locate/neuroimage

Group-level cortical and muscular connectivity during perturbations to walking and standing balance

Steven M. Peterson [a,*], Daniel P. Ferris [b]

[a] Department of Biomedical Engineering, School of Engineering, University of Michigan - Ann Arbor, MI, USA
[b] J. Crayton Pruitt Family Department of Biomedical Engineering, University of Florida, Gainesville, FL, USA

ARTICLE INFO

Keywords:
Electroencephalography
Virtual reality
Independent component analysis
Balance perturbation
Effective connectivity

ABSTRACT

Maintaining balance is a complex process requiring multisensory processing and coordinated muscle activation. Previous studies have indicated that the cortex is directly involved in balance control, but less information is known about cortical flow of signals for balance. We studied source-localized electrocortical effective connectivity dynamics of healthy young subjects (29 subjects: 14 male and 15 female) walking and standing with both visual and physical perturbations to their balance. The goal of this study was to quantify differences in group-level corticomuscular connectivity responses to sensorimotor perturbations during walking and standing. We hypothesized that perturbed visual input during balance would transiently decrease connectivity between occipital and parietal areas due to disruptive visual input during sensory processing. We also hypothesized that physical pull perturbations would increase cortical connections to central sensorimotor areas because of higher sensorimotor integration demands. Our findings show decreased occipito-parietal connectivity during visual rotations and widespread increases in connectivity during pull perturbations focused on central areas, as expected. We also found evidence for communication from cortex to muscles during perturbed balance. These results show that sensorimotor perturbations to balance alter cortical networks and can be quantified using effective connectivity estimation.

1. Introduction

In real world scenarios, humans frequently make postural adjustments to avoid losing balance. Such adjustments necessitate precise coordination between sensory input, cognitive processing, and motor control (Macpherson and Horak, 2012). Despite the cortex's involvement in maintaining balance (Bolton, 2015), our current understanding of real-world human cortical activity during balance perturbations remains limited (Varghese et al., 2017). Stationary recordings and low temporal resolution have limited traditional neuroimaging methods, such as functional magnetic resonance imaging (fMRI) and functional near-infrared spectroscopy (fNIRS). In contrast, high-density, source-localized electroencephalography (EEG) is a promising method to assess human cortical dynamics during balance because of its high temporal resolution and portability (Gramann et al., 2014, 2011). While EEG can be limited by low spatial resolution and artifact contamination (Macpherson and Horak, 2012), blind-source separation techniques such as independent component analysis can separate out cortical activity from artifacts, leading to enhanced spatial resolution and reduced artifact contamination (Gwin et al., 2010; Makeig et al., 1996; Wagner et al., 2012).

Because a response to perturbed balance involves coordination amongst multiple sensory systems, it is important to study the flow of information across the multiple cortical areas that process and integrate these senses. Balance control involves sensory inputs from visual, vestibular, and proprioceptive sensory systems (Macpherson and Horak, 2012), and damage to any of them can seriously impair balance (Collings et al., 2015; Janssens et al., 2013; Nuti et al., 2016). A quantitative measure of the cortical networks involved in this multisensory integration during perturbed balance responses could be useful for assessing the effects of aging on balance and could also help assess the severity of motor impairments such as freezing of gait, which has been linked to sensory cues (Hallett, 2008). In addition, the cortex appears to dynamically weight information based on its utility for the current task (Hwang et al., 2014; Oie et al., 2002), which is known as sensory reweighting. EEG studies have identified several sensorimotor cortical regions with increased activity during perturbed balance (Sipp et al., 2013; Slobounov et al., 2009), along with evidence that cortical information flow is

* Corresponding author. Box 351800, University of Washington, Seattle, WA, 98195-1800, USA.
E-mail address: stepeter@uw.edu (S.M. Peterson).

https://doi.org/10.1016/j.neuroimage.2019.05.038
Received 29 January 2019; Received in revised form 15 May 2019; Accepted 15 May 2019
Available online 18 May 2019

modulated by such perturbations (Varghese, 2016). Connectivity analysis using Granger causality can be used to quantify this information flow amongst sources, assessing directional information flow because of EEG's high temporal resolution (Blinowska, 2011). Such connectivity analyses can use source-localized EEG components, which are less susceptible to motion artifact and volume conduction than channel data (Brunner et al., 2016; Snyder et al., 2015). Using connectivity analyses, studies have uncovered altered cortical information flow patterns across various motor tasks (Kline et al., 2016; Rowe et al., 2002) and due to motor impairments (Liu et al., 2016; Shine et al., 2013). Connectivity analysis of cortical information flow during balance perturbations can enhance our understanding of how the human cortex integrates multisensory information and generates an appropriate postural response.

Previous studies have shown that cortico-cortical and cortico-muscular connectivity patterns change between motor tasks and when balance is perturbed. Cortico-cortical connectivity increases during standing compared to treadmill walking, but decreases during standing when performing a cognitive task, suggesting increased attention during stationary balance control compared to walking (Lau et al., 2014). For expected and unexpected balance perturbations, connectivity response patterns were found to be similar, although connectivity strengths were higher during unexpected perturbations (Varghese, 2016). Another study showed that balance perturbation connection patterns differed across frequency bands, with a theta network (5–7 Hz) in fronto-centro-parietal cortical regions and an alpha network (9–11 Hz) in occipito-parietal areas (Mierau et al., 2017). This indicates that analyzing connectivity across frequencies may be particularly useful when analyzing connectivity patterns. In addition to cortico-cortical connections, multiple studies have found evidence for corticomuscular connectivity during gait (Artoni et al., 2017; Petersen et al., 2012; Roeder et al., 2018). For perturbed balance responses, subcortical areas have been thought to primarily drive the postural response (Jacobs and Horak, 2007), but it is unclear if cortical areas are directly involved in muscle responses. While balance perturbations may involve fewer anticipatory balance responses compared to gait, similar connectivity patterns between unexpected and expected balance perturbations were seen by Varghese (2016). In general, many aspects of connectivity during perturbed balance remain unexplored (Varghese et al., 2017), especially when analyzing source-localized EEG.

The purpose of this study was to quantify differences in cortical and muscular connectivity patterns to brief sensorimotor perturbations that challenged postural control during walking and standing. For balance perturbations, we used a 20-degree field-of-view rotation or a pull at the waist. We hypothesized that this rotation perturbation would transiently decrease connectivity between occipital and parietal areas compared to baseline, due to disruptive visual information negatively influencing stability. Such decreased connectivity would provide evidence for sensory reweighting during the rotation perturbations. We also hypothesized increased perturbation-evoked connectivity in central sensorimotor cortical areas during pull perturbations, as more sensorimotor integration and attention is needed. This is supported by previous perturbation-evoked EEG activity being located to central cortical areas (Sipp et al., 2013; Varghese et al., 2014). Additionally, we performed connectivity analysis across two frequency bands and expected that it might provide extra information not seen in time-domain connectivity analysis, similar to the differences between time-frequency and time-domain spectral power analyses of cortical sources (Peterson and Ferris, 2018a).

2. Materials and methods

We tested 30 healthy, young adults [15 females and 15 males, age 22.5 ± 4.8 years (mean ± SD {standard deviation})]. We discarded one male subject's data in post-processing. All subjects identified themselves as right hand and right foot dominant, with normal or corrected vision. We screened subjects for neurological, orthopedic, or cardiac conditions and injuries. All subjects provided written informed consent. The University of Michigan Health Sciences and Behavioral Sciences Institutional Review Board approved our protocol for the protection of human subjects. Prior to testing, we prescreened all subjects for motion sickness in virtual reality.

During the experiment, subjects either walked at 0.22 m/s or stood on a 2.5 cm tall by 12.7 cm wide balance beam mounted to a treadmill. The beam was only wide enough for one foot to enforce tandem gait and tandem stance. Subjects wore a body-support harness for safety, with extended support straps to allow unrestricted mediolateral movement. We instructed subjects to look straight ahead and avoid looking down at their feet. We also instructed subjects to cross their arms to increase the difficulty of the task and to decrease inter-subject variability because there is no variation in arm movement. Subjects were also told to walk heel-to-toe and move their hips side-to-side to balance, avoiding rotations across their body's longitudinal axis. These instructions align with previous treadmill balance beam walking studies (Domingo and Ferris, 2010, 2009; Sipp et al., 2013).

We presented subjects with two types of sensorimotor perturbations: a side-to-side pull at the waist and a 20-degree field-of-view rotation (Fig. 1). The side-to-side pull was performed using rotational motors on either side of the subject. During perturbation onset, one motor rotated a bar away from the subject. This bar was fixed to a wire attached to the subject, pulling the subject mediolaterally to one side. The perturbation lasted for 1 s before the motor rotated back to its starting position. We used tensile load cells in series with the wire connected to the subject in order to determine the pull perturbation onsets. The field-of-view rotation was performed using a virtual reality headset (Oculus Rift DK2, Oculus, Redmond, WA) with an attached webcam (Logitech c930e, Logitech, Lausanne, Switzerland). The webcam view was displayed on the virtual reality headset, providing subjects a pass-through virtual reality experience. We performed perturbations by digitally rotating the virtual reality view 20° clockwise or counterclockwise. This rotation occurred immediately from 0 to 20°, lasting for a half second before the virtual reality view returned to its starting position. Subjects were exposed to one perturbation type while either tandem walking or tandem standing on the balance beam. The two perturbation types (pulls, rotations) and two physical tasks (walking, standing) resulted in four

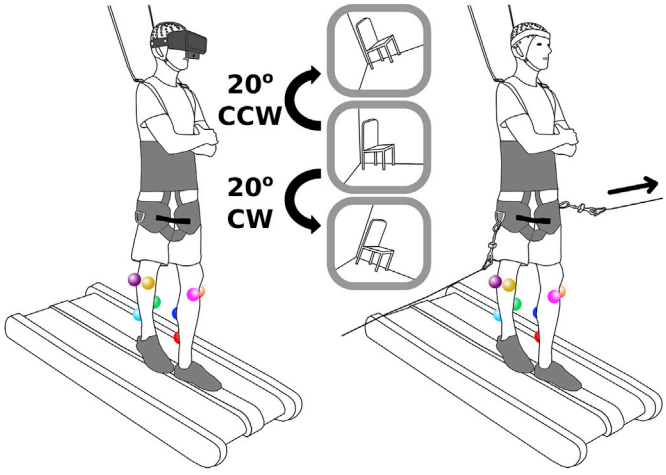

Fig. 1. Sketch of the two perturbation types. During the experiment, subjects were physically or visually perturbed while either walking or standing on a treadmill-mounted balance beam. During the rotation perturbations (left), subjects wore a virtual reality headset and had their field of view briefly rotated 20° clockwise or counterclockwise. Pull perturbations (right) involved a brief, mediolateral tug at the subject's waist. Colored dots denote approximate EMG placements at 8 lower leg muscles: left tibialis anterior (pink), left peroneus longus (orange), left medial gastrocnemius (blue), left soleus (red), right tibialis anterior (yellow), right peroneus longus (purple), right medial gastrocnemius (green) and right soleus (cyan).

conditions. Each condition lasted 10 min, and subjects experienced 150 perturbations (75 per side, randomized). Perturbation timings were randomly spaced 4.0 ± 0.6 s (mean ± SD) apart for all 4 conditions.

We recorded 136-channel EEG (BioSemi Active II, BioSemi, Amsterdam, NL) and 8 lower-leg electromyography (EMG) channels (Vicon, Los Angeles, CA). EEG was sampled at 512 Hz and synced with visual perturbations using Lab Streaming Layer (Delorme et al., 2011). EEG electrode positions were determined using a Zebris ELPOS digitizer (Zebris Medical GmbH, Isny, Germany). We recorded EMG from 4 lower leg muscles on each leg: tibialis anterior, soleus, medial gastrocnemius, and peroneus longus (Biometrics, Ladysmith, VA). Fig. 1 shows approximate EMG placements. EMG was sampled at 1000 Hz and was recorded with the load cell data. We synchronized the EMG and EEG data using a 0.5 Hz square wave. To determine pull perturbation onsets, we detrended the load cell data (LCM703, OMEGA Engineering, INC., Norwalk, CT) and used a 3-standard deviation threshold from baseline activity that was visually inspected.

We used custom EEGLAB 13.5.4b scripts to process the EEG data (Delorme and Makeig, 2004), as shown in Fig. 2. EEG data was downsampled to 256 Hz, high-pass filtered at 1 Hz, merged across all conditions, and referenced to the median channel value for each timepoint. We reduced 60 Hz line noise using the EEGLAB Cleanline plugin (Mullen, 2014). We rejected bad channels that had abnormally high standard deviation, had kurtosis above 5 standard deviations, or were uncorrelated from all other channels ($r < 0.4$) for more than 1% of the total time (Peterson and Ferris, 2018a). We retained 111 ± 7 channels (mean ± SD) across all subjects. These remaining channels were further denoised. We removed large mechanical artifacts using artifact subspace reconstruction (Mullen et al., 2013), setting a threshold of 20 standard deviations (Artoni et al., 2017). We also performed selective low-pass filtering by combining ensemble empirical mode decomposition (Al-Subari et al., 2015; Wu and Huang, 2009) and canonical correlation analysis (Hotelling, 1936). This targeted large high-frequency activity with low autocorrelation, such as muscle activity and line noise (Safieddine et al., 2012), to limit the influence of such artifacts on the independent component analysis decompositions. See Peterson et al. (2018) for further details. We then performed a common average reference and interpolated the rejected channels to maintain a consistent head montage.

We performed adaptive mixture independent component analysis (Palmer et al., 2008, 2006), reducing down to 80 principal components prior to independent component analysis to keep the data at full rank. We performed dipole fitting on each resulting independent component, only retaining components that were well fit by the model (residual model variance <15%). We visually inspected the remaining dipoles, removing components contaminated with muscle artifact, eye movements, and line noise based on power spectra and dipole location. The final cortical components were pooled across all subjects and grouped with k-means clustering. We retained clusters containing more than half of the subjects (>15), resulting in the 8 cortical clusters (Fig. 3). One subject with dipoles in only 2 clusters was removed to avoid underfitting the model for connectivity estimation later on. Cortical clusters were left occipital (18 subjects), right occipital (16 subjects), left sensorimotor (23 subjects), anterior cingulate (16 subjects), right sensorimotor (22 subjects), posterior parietal (22 subjects), supplementary motor area (26 subjects), and anterior parietal (18 subjects). If a subject had multiple dipoles in one cluster, we retained the dipole with the largest variance. This resulted in 5.6 ± 1.8 cortical dipoles per subject (mean ± SD). We split the data into epochs of −1 to 2 s, centered around perturbation onset, resulting in 146 ± 1 epochs for stand pull, 145 ± 5 epochs for walk pull, 144 ± 9 epochs for stand rotate, and 146 ± 1 epochs for walk rotate (mean ± SD). We discarded epochs when either EEG or EMG data had a gap in recording. No other epoch rejection was performed.

We also included data from the 8 lower leg EMG electrodes in our connectivity analysis. EMG data was 1 Hz high-pass filtered and full-wave rectified as has been done previously (Gwin and Ferris, 2012; Raez et al., 2006). We then downsampled EEG and EMG data to 128 Hz and synchronized them together, using epochs of −1 to 2 s, centered around perturbation onset. Every subject had data from all 8 muscles, increasing each subject's number of corticomuscular signals for connectivity analysis by 8.

We used the source information flow toolbox (SIFT) to fit a multivariate autoregressive model to each subject's data (Delorme et al., 2011). We used a sliding window of 400 ms with step size of 20 ms. For each subject's autoregressive model, we selected a model order of 32, which provided a frequency resolution of 4 Hz (Cohen, 2014). To check if the models were overfitting the data, we also performed connectivity estimation using model orders of 9, based on the minimum Hannan-Quinn information criteria rounded up to the nearest integer model order when looking at lower model orders between 1 and 15.

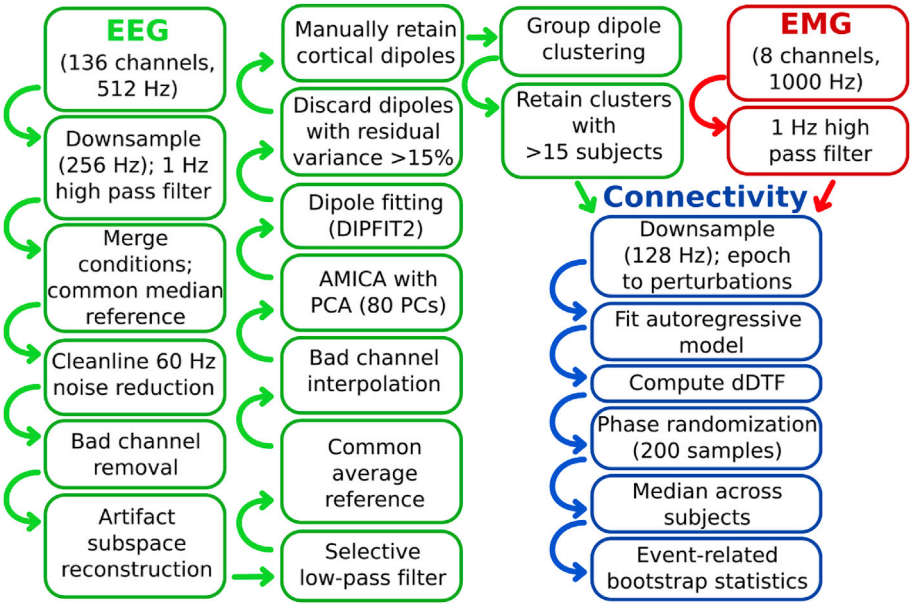

Fig. 2. Schematic of processing pipeline. The EEG (green) and EMG (red) preprocessing steps are shown, along with the corticomuscular connectivity estimation (blue).

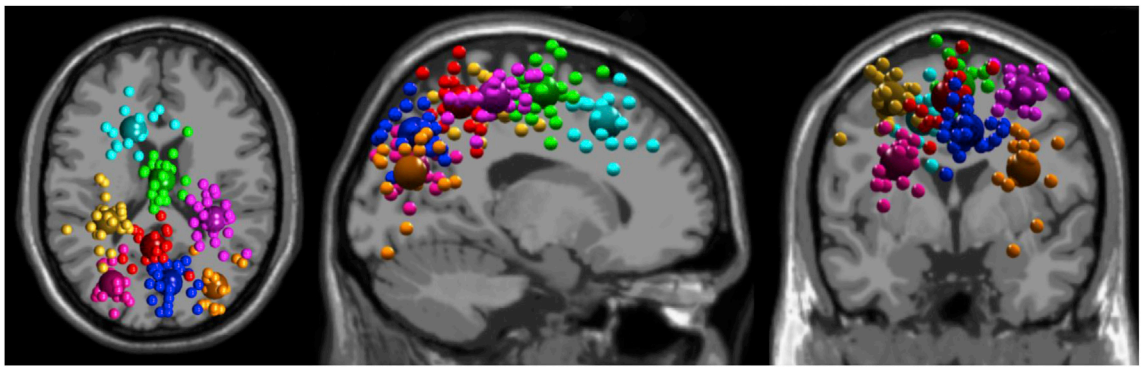

Fig. 3. Cortical cluster locations. Cortical dipole locations for all 29 subjects are shown after retaining at most one dipole per cluster per subject. Dipoles are colored according to the 8 identified cortical clusters: left occipital (pink), right occipital (orange), posterior parietal (blue), anterior parietal (red), left sensorimotor (yellow), right sensorimotor (purple), supplementary motor area (green), and anterior cingulate (cyan). Large dots denote each cluster centroid.

However, we selected a model order of 32 for our main analysis to achieve the necessary spectral resolution of 4 Hz. We then correlated the cortical connectivity results from the high and low order models for each subject. We also plotted the multiple information criteria (Lütkepohl, 2007b) across subject models for model order from 1 to 40. We validated our high-order fitted model using tests in SIFT for consistency, stability, and whiteness of residuals. Consistency was determined by simulating data from the model and calculating the Euclidean norm between the real and simulated data correlation matrices (Ding et al., 2000a). These values range from 0 to 100%. Higher consistency indicates that the model adequately captures the correlation structure of the real data. Stability was determined checking the logarithm of the largest eigenvalue of the model coefficient matrix (Ding et al., 2000b). For negative values, the model is considered stable and the results are stationary across time. Whiteness of residuals was tested using an autocorrelation function test with confidence intervals, where the final value indicates the probability that the data is white. This value ranges from 0 to 1 and should be as high as possible to increase the confidence that the residuals are truly white. If the residuals are not white, then this would indicate that there is still some correlation structure in the data that is not captured by the model (Lütkepohl, 2007b).

Next, we estimated connectivity using direct directed transfer function (dDTF). Directed transfer function can be considered an extension of Granger causality (Granger, 1969; Kamiński et al., 2001) that can determine directed multichannel information flow. To minimize the effects of indirect connections, dDTF involves multiplying full frequency directed transfer function by partial coherence, which is sensitive to only direct connections (Korzeniewska et al., 2003). We chose dDTF to quantify connectivity based on its robust performance and ability to ignore indirect connections (Astolfi et al., 2007; Höller et al., 2017; Peterson and Ferris, 2018b). We calculated dDTF across 30 logarithmically-spaced frequency bins ranging from 4 to 50 Hz and 244 linearly-spaced time bins from −1.4–2.4 s, with perturbation onset at 0 s. After connectivity estimation, we focused on −0.5–1.5 s. To minimize false positive connectivity values, we applied phase randomization statistics to each subject's dDTF connectivity results (Theiler et al., 1992), using 200 samples per subject and setting non-significant differences to 0. This was done separately for each subject. For each surrogate sample, the input data's phase is randomized, and then model fitting and connectivity estimation are performed, creating a null distribution. Within each subject, the connectivity results with non-randomized phase can be compared with the phase-randomized null distribution to determine how likely they reflect true connectivity. After phase randomization, we took the median dDTF value across subjects at each time-frequency point at each connection, including only the subjects that had each connection. We used the median to avoid a single subject from skewing the results. This is similar to the region of interest analysis used by Artoni et al. (2017).

In addition to dDTF, we also computed spectral density for each subject's autoregressive model, using phase randomized surrogate statistics and then averaging across subjects. We applied bootstrap statistics (200 samples) to determine significantly different connectivity from the half second of activity prior to perturbation onset (Efron and Tibshirani, 1993). This half-second of baseline activity was subtracted off and all non-significant differences from baseline were set to 0. We then plotted the resulting spectral density time-frequency maps, known as event-related spectral perturbation (ERSP) plots. Note that our ERSPs use model-fitted results instead of the data directly. We generated ERSPs across cortical clusters for both perturbation types. We also plotted ERSPs for the 8 lower leg muscles during the pull perturbations only. We focused only on the 2 pull perturbation conditions for muscle activity due to the rotations having minimal perturbation-evoked intermuscular connectivity, which matches our previous findings (Peterson and Ferris, 2018a).

We split our estimated connectivity results into baseline and event-related components, similar to EEG spectral power analyses. This assessed the same connectivity results in two different ways to tease apart baseline effects from each condition and perturbation-specific, event-related effects. Baseline connectivity was averaged from −0.5–1.5 s around perturbation onset. We further averaged these values across predefined frequency bands: theta (4–8 Hz), alpha (8–13 Hz), and all (4–50 Hz). These average values were then averaged up for each connection, with self-connections discarded. We then performed two-way ANOVA tests across subjects for each connection, analyzing the effects of physical task (standing v. walking) and perturbation type (pull v. rotation). P-values were corrected for multiple comparisons using false discovery rate (Benjamini and Yekutieli, 2001).

To obtain event-related connectivity, we performed the same half-second baseline subtraction and bootstrap statistics as was done for the ERSPs. For corticomuscular connectivity, we added extra bootstrap significance masking for non-significant differences between cortex-to-muscle and muscle-to-cortex in corresponding connections. However, we do not show the connectivity time-frequency plots here because we had 240 connections and 4 conditions. Instead, average event-related connectivity during the 1 s following perturbation onset is visualized using chord diagrams, averaged into theta (4–8 Hz) and alpha (8–13 Hz) frequency bands (see Fig. S1 for an example chord diagram). Chord diagrams have been previously used to visualize connectivity (Caldwell et al., 2017; Gu et al., 2014). For each averaged connection, we performed a *t*-test across subjects ($p < 0.05$) to determine which connections were consistently above or below 0 and grayed out the non-significant connections on the chord diagrams. Similar to the ERSPs, we focused only on the pull perturbation conditions for intermuscular and corticomuscular connectivity. All statistical tests and chord diagrams were computed in R (R Core Team, 2017).

Table 1
Model fitting results.

	Stand Pull	Walk Pull	Stand Rotate	Walk Rotate
Parameter to datapoint ratio	0.80 (0.21)	0.88 (0.38)	0.82 (0.24)	0.80 (0.21)
Residual whiteness likelihood	0.91 (0.01)	0.90 (0.01)	0.91 (0.01)	0.90 (0.01)
Consistency (%)	49.4 (2.4)	43.9 (4.9)	49.9 (2.9)	49.5 (2.9)
Stability index	−0.15 (0.00)	−0.15 (0.01)	−0.15 (0.00)	−0.15 (0.00)

Average validation results from model fitting are shown for all 4 conditions, with standard deviation in parentheses. We fixed the model order at 32 for all models to allow for appropriate frequency resolution down to 4 Hz. Residual whiteness was tested using the autocorrelation function test for significance. Consistency indicates how well the model can generate data that correlates to the original data, with 100% being a perfect match. Stability index looks at how stationary the model is across time. The model can be considered stable if the stability index is less than 0.

We also wanted to quantify how the number of connections between cortical areas varies with the number of subjects available, which could be useful in determining the optimal number of subjects needed for similar connectivity analyses. Group connectivity analysis can be challenging because the number of connections scales quadratically with the number of independent components available. Because independent component analysis is data-driven, it can be challenging to determine the relationship between number of samples per connection and number of subjects. To assess this on our data, we performed 200 bootstrap samples of our 29 subjects for subject numbers ranging from 1 to 29. We then performed a quadratic fit on the maximum, mean, and minimum number of samples across all edges using a least squares model in R (R Core Team, 2017).

3. Results

3.1. Model validation

Our model validation metrics indicate that the multivariate autoregressive models for each condition fits its respective subject's data reasonably well (Table 1). The model order for all conditions was set to 32 to obtain frequency resolution down to 4 Hz. When we compared each subject's estimated cortico-cortical connectivity to a lower model order (9), we obtained a correlation coefficient of 0.86 ± 0.32 (mean $\pm$ SD). The subject-averaged connectivity patterns were also visually similar for both model orders. This suggests that a model order of 32 did not notably overfit the data, despite a consistent parameter to datapoint ratio over 0.8 across subjects and conditions, which was above the target value of 0.1 to avoid overfitting. Additionally, all information criteria measures we used decreased for a model order of 32 compared to lower model orders (Fig. S2), suggesting that 32 was a reasonable model order. The residual whiteness likelihood was 0.905 on average for all subjects and conditions, indicating that there is an 9.5% chance that the residuals are not white. While this would ideally be 95% or higher, this likelihood did not increase with higher model orders, indicating that this is a reasonable model order. Consistency was ~44–50% across conditions, likely indicating that there is still some variance in the data that the model does not capture. However, all conditions had model stability index values below 0, indicating that all models were stable.

We also tested the effect of artifact subspace reconstruction, finding minimal impact on connectivity estimation. Despite not affecting connectivity estimation at similar thresholds in other studies (Artoni et al., 2017; Chang et al., 2018), artifact subspace reconstruction has unclear effects that may change based on the data used. We computed connectivity on 2 subjects without using artifact subspace reconstruction, using a 1 mV threshold to remove bad trials. We used the same independent component weights and model order (32) to facilitate a straightforward comparison. For each cortico-cortical connection, we computed correlation between estimated dDTF with artifact subspace reconstruction and without. EMG was not processed with artifact subspace reconstruction, so we focused on cortico-cortical connections only. Cortico-cortical correlation values between the 2 subjects with and without artifact subspace reconstruction were 0.99 ± 0.00 (mean $\pm$ SD). Based on this, artifact subspace reconstruction did not appear to affect our connectivity results.

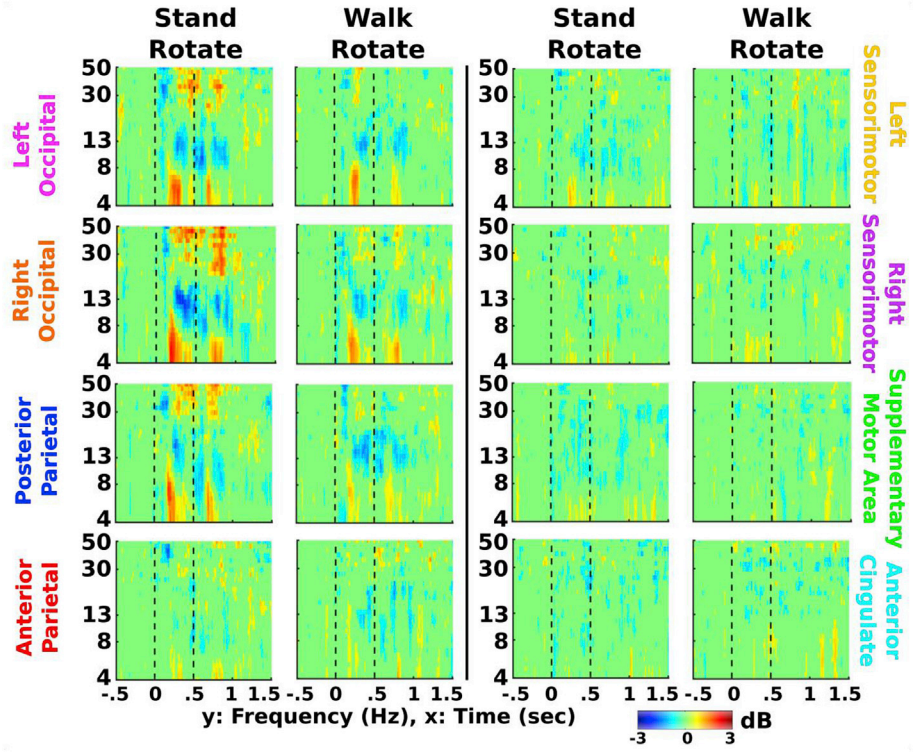

Fig. 4. Cortical event-related spectral perturbations (ERSPs) to visual rotations. EEG spectral power modulations to rotation perturbations are shown during standing and walking conditions. Results were generated from the fitted models for each subject, instead of averaging across trials. We subtracted out baseline activity during the half-second before perturbation onset. Red indicates increased spectral power compared to baseline, known as synchronization, while blue reflects a decrease in spectral power relative to baseline, known as desynchronization. We set non-significant differences from baseline to 0 ($p > 0.05$). Vertical dashed lines indicate perturbation onset at 0 s and offset at 0.5 s. We found distinct spectral patterns in theta (4–8 Hz), alpha (8–13 Hz), and low gamma (30–50 Hz), primarily in occipital and posterior parietal areas.

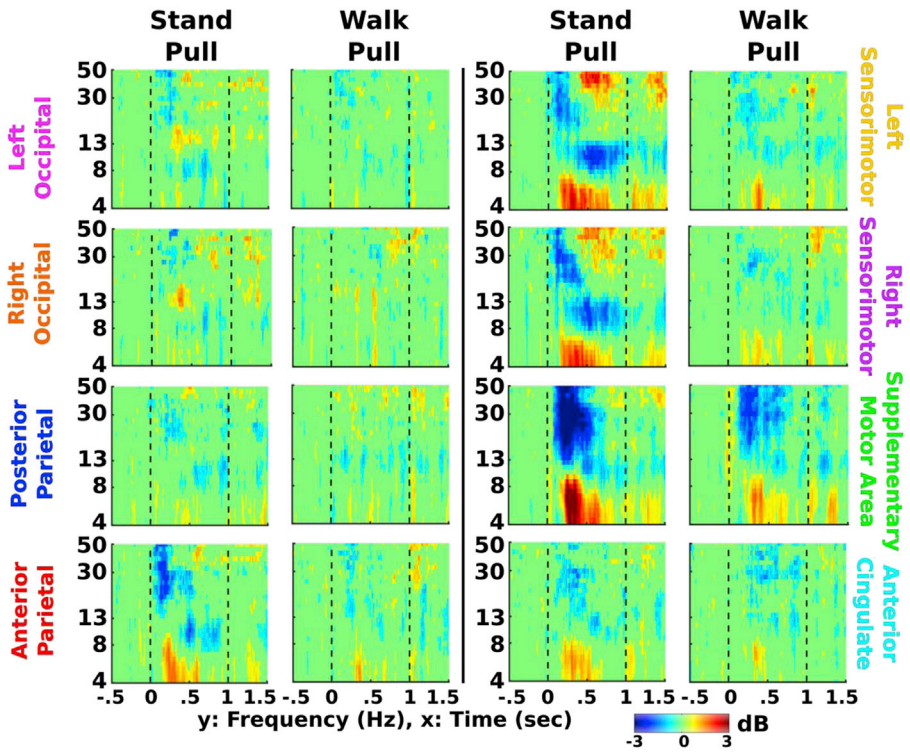

Fig. 5. Cortical event-related spectral perturbations (ERSPs) to physical pulls. EEG spectral power modulations to pull perturbations are displayed during standing and walking conditions using fitted models for each subject. We subtracted out the half-second before perturbation onset as a baseline. Red indicates increased spectral power compared to baseline, or synchronization, while blue reflects decreased spectral power relative to baseline, or desynchronization. We zeroed out all non-significant differences from baseline ($p > 0.05$). Vertical dashed lines indicate perturbation onset at 0 s and offset at 1 s. We found similar synchronization/desynchronization patterns to the visual perturbations, but primarily located in central motor areas.

3.2. Perturbation-evoked spectral power

Cortical ERSPs showed consistent patterns of theta (4–8 Hz) synchronization followed by alpha/beta (8–30 Hz) desynchronization, along with variations in low gamma power (30–50 Hz). This pattern occurred in left/right occipital and posterior parietal areas for visual rotations (Fig. 4), but occurred in anterior parietal, left/right sensorimotor, supplementary motor area, and anterior cingulate for pull perturbations (Fig. 5). For both perturbation types, ERSPs visually appear to be stronger during standing compared to walking, indicating a difference in sensorimotor processing between the two physical tasks.

For the lower leg muscles, we found a 4–13 Hz power increase following pull perturbation onset, along with a brief 20–50 Hz power decrease (Fig. 6). The low-frequency power increase during standing

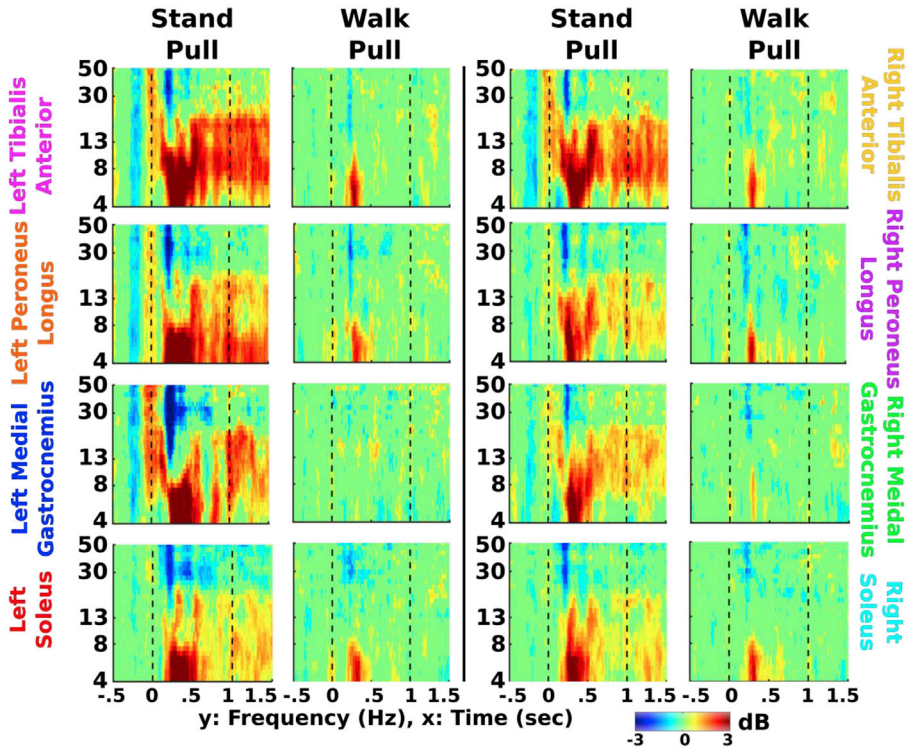

Fig. 6. Muscular event-related spectral perturbations (ERSPs) to physical pulls. Lower leg EMG spectral power fluctuations to pull perturbations are shown during standing and walking conditions, after averaging fitted model results across subjects. We subtracted out the half-second before perturbation onset as a baseline. Red indicates an increase in spectral power compared to baseline, while blue reflects decreased spectral power relative to baseline. We zeroed out any non-significant differences from baseline ($p > 0.05$). Vertical dashed lines indicate perturbation onset at 0 s and offset at 1 s. EMG ERSPs show increased magnitude from walking to standing across all muscles recorded from, particularly for both medial gastrocnemius muscles.

persisted throughout the 1.5 s after perturbation onset. Similar to the cortical ERSPs, spectral fluctuations during standing appeared visually stronger compared to walking.

3.3. Baseline connectivity

Baseline connectivity during standing conditions showed increased cortico-cortical alpha connectivity (8–13 Hz) and intermuscular connectivity between legs (inter-leg) compared with walking (Fig. 7A). For cortico-cortical connections, we found significant effects of physical task for both alpha and all (4–50 Hz) frequency bands ($p = 2.0e\text{-}7$ and 0.02, respectively), reflecting increased connectivity during standing compared to walking. Alpha band connectivity also had a significant effect of perturbation type, with connectivity during pull perturbation increased compared to rotations. This effect was not seen in the theta and all frequency bands, illustrating the utility of splitting up connectivity results into separate frequency bands. For intermuscular connectivity (Fig. 7B), we found a significant effect of intra-leg vs. inter-leg connectivity for theta (4–8 Hz), alpha, and all frequency bands during pull perturbations ($p = 5.8e\text{-}10$, 5.5e-11, and 2.7e-10, respectively), with intra-leg connectivity strength consistently increased in magnitude compared to inter-leg. We expected that muscles within each leg would coordinate more than muscles between legs. Using a *t*-test comparison, we found a significant ($p < 0.05$, false discovery rate correction) increase in all inter-leg connectivity frequency band strengths during standing compared to walking ($p = 1.1e\text{-}6$, 5.6e-8, and 1.1e-6, respectively). In contrast, we found no significant differences in intra-leg connectivity strengths between standing and walking (theta: $p = 0.30$, alpha: $p = 0.51$, all: $p = 0.30$). For baseline corticomuscular connectivity (Fig. 7C), we found significant effects for all frequency band of physical task (theta: $p = 1.1e\text{-}19$, $p = 0.04$, $p = 4.2e\text{-}19$) and directionality (theta: $p = 1.4e\text{-}33$, alpha: $p = 2.0e\text{-}40$, all: $p = 1.2e\text{-}61$). This reflects an increase in corticomuscular connectivity during walking compared to standing and a large increase in cortex-to-muscle connectivity compared to muscle-to-cortex.

3.4. Perturbation-evoked connectivity patterns

For cortico-cortical connectivity, we found that pull perturbations during standing transiently increased theta connectivity in central motor areas, while rotation perturbations during standing decreased alpha connectivity between parietal and occipital areas (Fig. 8). During pull perturbations while standing, theta connectivity significantly increased between the supplementary motor area and left/right sensorimotor, anterior parietal, anterior cingulate, and right occipital areas. Theta connectivity also increased between left and right sensorimotor areas. For pull perturbations while standing, supplementary motor area appears to be a hub of theta connectivity with motor areas. During pull perturbations while walking, most of the significant connections during stance disappear, except between supplementary motor area and anterior cingulate. For rotation perturbations while standing, alpha connectivity significantly decreased following perturbation onset between left occipital and left sensorimotor, right occipital and right sensorimotor, and anterior parietal and posterior parietal. In all 3 cases, these occipito-parietal regions are located near each other (see Fig. 3). Similar to the pull perturbation results, these alpha connectivity decreases while standing do not appear during walking, indicating that cortical network activity to sensorimotor perturbations varies based on physical task.

For perturbation-evoked intermuscular connectivity, theta and alpha connectivity increased following pull perturbation onset (Fig. 9). Similar to baseline intermuscular connectivity, the perturbation-evoked inter-leg connectivity pattern appears more pronounced during stance compared to perturbations while walking. During walking, the significant connectivity increases occurred primarily between peroneus longus and soleus muscles on either leg. In contrast, all muscles show increased theta and alpha connectivity during pull perturbations while standing, but with visually stronger connections for left leg muscles compared to the right leg, especially for theta connectivity in left medial gastrocnemius and left soleus compared to their right leg counterparts.

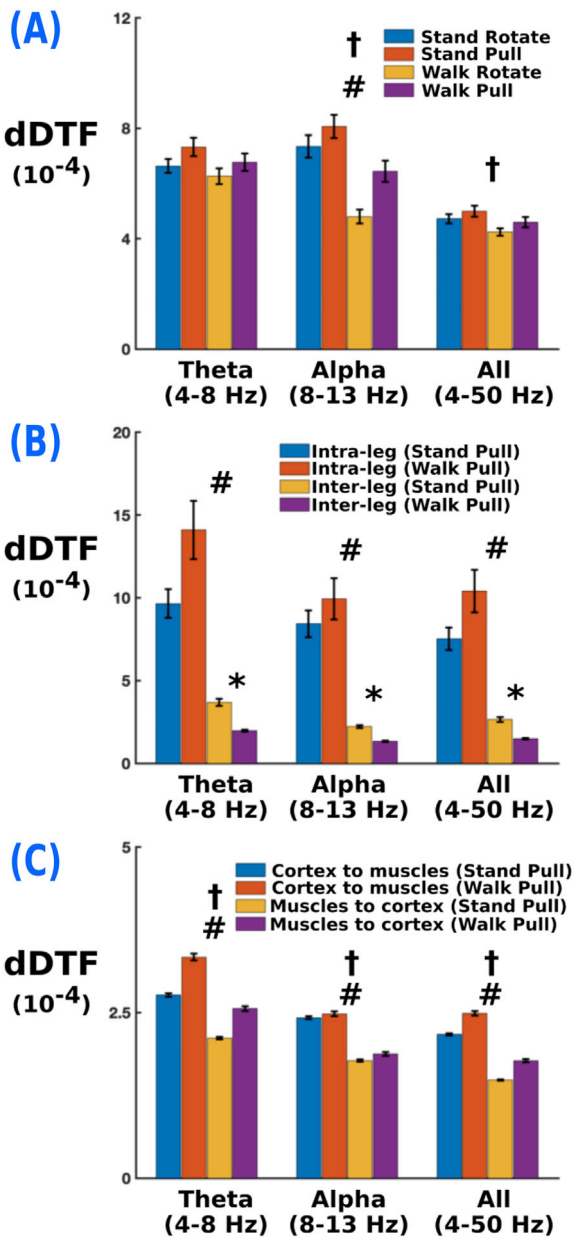

Fig. 7. Baseline connectivity results. Plots show mean baseline (A) cortical, (B) muscular, and (C) corticomuscular connectivity with standard error bars. Results were assessed using a two-way ANOVA with false discovery rate correction for multiple comparisons (# means significant effect of (A) perturbation, (B) inter/intra-leg, or (C) corticomuscular connectivity direction; † indicates significant effect of physical task, $p < 0.05$). Asterisk in (B) indicates significant difference ($p < 0.05$, with false discovery rate correction) in inter-leg muscular connectivity between stand pull and walk pull conditions. Cortical alpha connectivity significantly decreased during walking compared to standing, inter-leg muscular connectivity significantly increased during standing compared to walking, and baseline cortex-to-muscle connectivity was significantly increased compared with muscle-to-cortex connectivity.

For perturbation-evoked corticomuscular connectivity, we found small but significant differences, mostly during standing (Fig. 10). For pull perturbations during stance, we found several transient increases in theta connectivity between cortical areas and lower leg muscles. Corticomuscular connections into the left medial gastrocnemius were

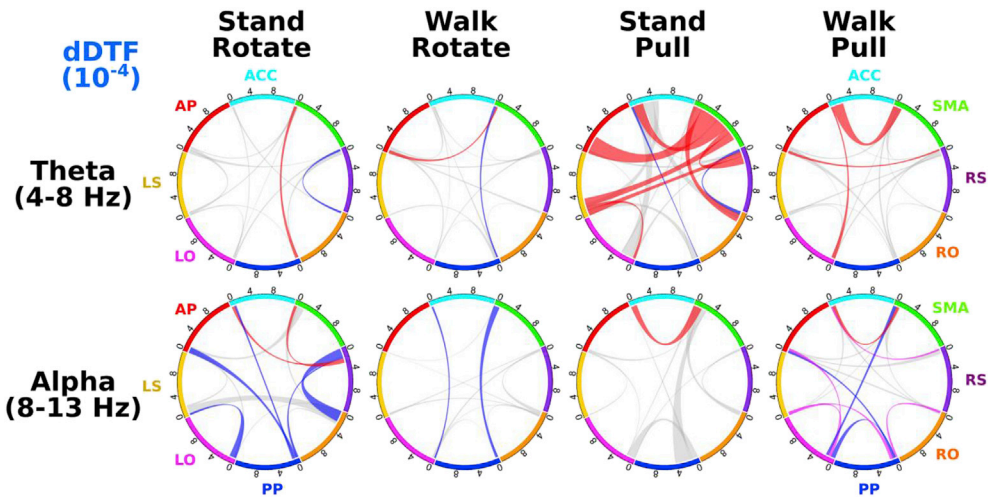

Fig. 8. Perturbation-evoked cortical connectivity. Chord diagrams show average cortico-cortical connection strengths during the 1 s after perturbation onset, after subtracting baseline activity during the half-second preceding perturbation onset. Cortical areas are left occipital (LO), right occipital (RO), posterior parietal (PP), anterior parietal (AP), left sensorimotor (LS), right sensorimotor (RS), supplementary motor area (SMA), and anterior cingulate (ACC). Red connections indicate significantly increased connectivity from baseline in both directions, blue ones indicate significantly decreased connectivity from baseline in both directions, and magenta ones denote one direction is significantly increased from baseline while the other direction is significantly decreased. Gray denotes non-significant connections. Each cortical area's arc segment is scaled from 0 to 12e-4. Alpha connectivity during stand rotate was decreased between nearby occipital (LO, RO, PP) and parietal (LS, RS, AP) areas. In stand pull, supplementary motor area was a hub of theta connectivity, with significant bidirectional connections between it and LS, AP, ACC, RS, and RO. The SMA and ACC connection persists during walk pull, but otherwise walking conditions have minimal similarities to the stand conditions.

particularly prominent compared to connections into the right medial gastrocnemius, with left medial gastrocnemius receiving connections from anterior cingulate, anterior parietal, and right occipital areas. Alpha connectivity during stance showed multiple significant decreases in corticomuscular connectivity compared to baseline from left occipital, posterior parietal, right sensorimotor, and anterior cingulate to left peroneus longus and from left sensorimotor to right medial gastrocnemius. Similar to cortico-cortical and intermuscular connectivity, event-related corticomuscular connectivity during walking was decreased compared to standing.

3.5. The impact of subject number on samples per connection

We found a predominantly linear relationship between number of samples per connection and number of subjects (Fig. S3). All quadratic best fit equations for the minimum, average, and maximum samples per connection were dominated by a significant linear term (Table S1). The average equation indicated that adding 2 subjects increased the average samples per connection by 1. This ratio likely differs across experiments due to factors such as experimental paradigm and quality of recordings. This linear trend indicates that source-space connectivity analyses can be performed with a reasonable number of subjects (e.g. ~20).

4. Discussion

We performed source-localized cortical and muscular connectivity analysis during sensorimotor perturbations that challenged balance, finding evidence for altered weighting of sensory information during cortical processing and directed corticomuscular connections during perturbed balance. Visual rotations during tandem standing notably decreased cortico-cortical alpha connectivity (8–13 Hz) between occipital and parietal areas, which supports our first hypothesis. In addition, pull perturbations while tandem standing increased theta (4–8 Hz) connectivity between supplementary motor area and central motor areas, as hypothesized, which may reflect increased sensorimotor processing and attention. We found significant directional corticomuscular connectivity, along with potential evidence of direct cortical influence on the muscular response to pull perturbations. Also, dividing baseline connectivity results into theta and alpha frequency bands provided more information than averaging across all frequencies, especially when assessing alpha connectivity.

4.1. Cortical spectral power and connectivity

We found similar cortical spectral fluctuation patterns following both perturbation types but localized in different cortical areas. Visual rotation perturbations primarily altered spectral power in occipital areas, while physical pull perturbations induced spectral fluctuations in central motor areas. This agrees with our previous results (Peterson and Ferris, 2018a). However, our previous results found no clear activity patterns at low gamma power (30–50 Hz), but our model-fitted results show a clear pattern (Figs. 4–5). These low gamma patterns do not appear to be artifact and may potentially reflect active cortical control, as has been seen for gamma power in electrocorticography (Miller et al., 2007). In addition, we did not find frontal cortical areas in our EEG source analysis. Connectivity in frontal areas has been shown to increase in older adults and in young adults when the postural task becomes more challenging (Huang et al., 2017). Our postural task may have been fairly easy to perform because it did not induce stepping, which may explain the lack of fronto-central clusters.

Baseline cortical alpha connectivity increased overall during standing compared to walking conditions. This increased alpha connectivity during standing compared to walking agrees with previous studies (Lau et al., 2014; Wagner et al., 2013). Likely because of this baseline connectivity difference across physical tasks, perturbation-evoked alpha spectral power patterns found during standing appeared mostly absent during walking conditions, which likely reflects a change in motor readiness (Wagner et al., 2014).

Perturbation-evoked cortical connectivity primarily showed theta band increases in central motor areas during stance pull perturbations compared to baseline connectivity and alpha band decreases between parietal and occipital areas during stance rotation perturbations

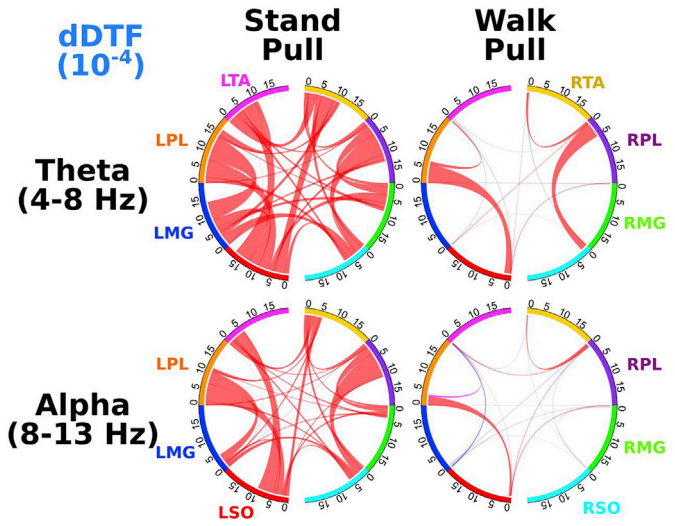

Fig. 9. Perturbation-evoked intermuscular connectivity. Chord diagrams show average intermuscular connection strengths during the 1 s following perturbation onset, after subtracting baseline activity during the half-second preceding perturbation onset. Lower leg muscles are left/right tibialis anterior (LTA/RTA), left/right peroneus longus (LPL/RPL), left/right medial gastrocnemius (LMG/RMG), and left/right soleus (LSO/RSO). Red connections indicate significantly increased connectivity from baseline in both directions, blue ones denote significantly decreased connectivity from baseline in both directions, and magenta ones indicate significantly increased connectivity from baseline in one direction with significantly decreased connectivity in the other direction. Gray denotes non-significant connections. Muscles in each diagram are split by left/right leg. Scale is 0 to 20e-4. Peroneus longus/soleus and tibialis anterior/peroneus longus connections persist across all conditions. Additionally, LMG and LSO show stronger incoming theta connections than RMG and RSO during stand pull.

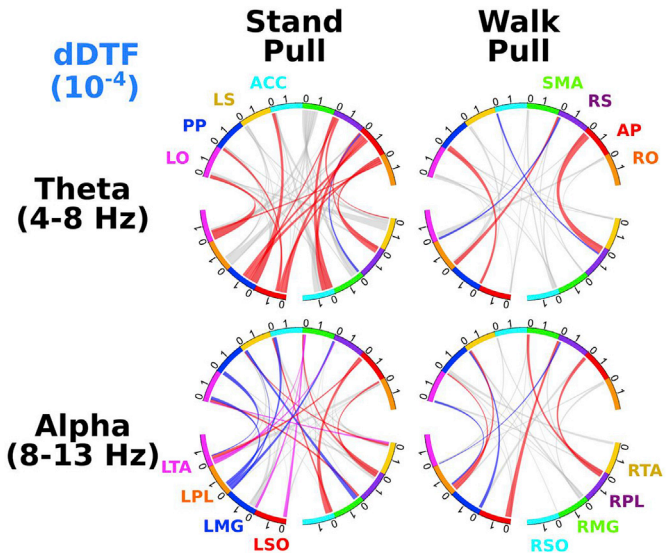

Fig. 10. Event-related corticomuscular connectivity. Chord diagrams show average corticomuscular connection strengths during the 1 s following perturbation onset, following baseline subtraction of the half-second preceding perturbation onset. Cortical sources are left occipital (LO), right occipital (RO), posterior parietal (PP), anterior parietal (AP), left sensorimotor (LS), right sensorimotor (RS), supplementary motor area (SMA), and anterior cingulate (ACC). Lower leg muscles are left/right tibialis anterior (LTA/RTA), left/right peroneus longus (LPL/RPL), left/right medial gastrocnemius (LMG/RMG), and left/right soleus (LSO/RSO). Red connections indicate significantly increased connectivity from baseline in both directions, blue ones denote significantly decreased connectivity from baseline in both directions, and magenta ones indicate one direction is significantly increased from baseline while the other direction is significantly decreased. Gray denotes non-significant connections. Only connections between muscles and cortical areas are displayed. Scale is only 0 to 2e-4. Overall, connectivity is stronger from the cortex to the muscles compared to the reverse direction. During stand pull, alpha connectivity decreased from baseline at LPL and between LS and RMG, while theta connectivity increased between LMG and RS, RO, AP, and ACC.

compared to baseline connectivity. While spectral density patterns also showed theta band increase and alpha band decrease relative to baseline, we were able to use connectivity analysis to formally determine how these cortical regions interact. This provides complementary information to spectral power. For example, occipital areas during standing rotation perturbations showed decreased alpha power (desynchronization). By analyzing connectivity, we found strong evidence that this alpha desynchronization is related to decreased alpha connectivity between occipital and parietal areas. This perturbation-evoked decrease in alpha connectivity between left/right sensorimotor and left/right occipital and between anterior and posterior parietal areas during visual rotations likely reflects unreliable visual input. We also found brief theta connectivity between supplementary motor area and other motor areas during pull perturbations while standing. Previous EEG balance studies have found large responses in supplementary motor area to perturbed balance (Solis-Escalante et al., 2018; Marlin et al., 2014; Varghese et al., 2014), and it seems to be a large hub of information flow during the stance pull perturbations. In addition, the strong theta connectivity between the supplementary motor area and anterior cingulate is relevant given previously found spectral power changes in the anterior cingulate during gait and proposed function as an error monitor (Carter et al., 1998; Gwin et al., 2011). Notably, this is the only significant theta band connection preserved during pull perturbations for both standing and walking conditions. This connectivity pattern did not appear during the rotation perturbations, potentially indicating that the anterior cingulate is more sensitive to physical errors than visual errors during balance. In contrast to theta and alpha connectivity, we found little beta (13–30 Hz) or low-gamma (30–50 Hz) baseline or perturbation-evoked corticomuscular connectivity, despite spectral power fluctuations in these bands for all conditions. Because of this, our connectivity analysis indicates that the alpha and beta desynchronization following perturbation onset reflect two distinct processes, highlighting the importance of using connectivity analysis in conjunction with spectral information.

4.2. *Intermuscular and corticomuscular connectivity during pull perturbations*

We found primarily low frequency (<13 Hz) connectivity among muscles, which was surprising because EMG and corticomuscular connectivity are usually analyzed at higher frequencies (Gwin and Ferris, 2012). Still, intermuscular coherence during balance control has been seen to be strongest at low frequencies (Boonstra et al., 2015, 2008) and is thought to reflect the activity of different muscles changing at the same time (Mochizuki et al., 2006). While this could be motion artifact, baseline connectivity within each leg is significantly larger than connectivity between legs, indicating that these results likely reflect true linkages amongst muscles. It has also been suggested that surface EMG recordings are low-pass filtered due to volume conduction by the skin (Farina and Holobar, 2016), which could lead to important information being located mostly at low frequencies.

For corticomuscular connections, we found that connections from the cortex to muscles were significantly increased compared to connections from muscles to cortex. This matches previous results during stereotyped walking by Artoni et al. (2017). Baseline corticomuscular connectivity also generally increased during walking compared to standing. We have previously shown that subjects are more unstable while walking during pull perturbations compared to standing (Peterson and Ferris, 2018a). However, perturbation-evoked corticomuscular connectivity was low in

magnitude and did not have a clear pattern. We have previously found that left medial gastrocnemius activity was strongest during pull perturbations while standing compared to walking and right medial gastrocnemius for both conditions (Peterson and Ferris, 2018a). Increased theta connectivity to left medial gastrocnemius from anterior cingulate, anterior parietal, and right occipital during stand pull (Fig. 10) may correspond to this increased muscle activity, but more research is needed to verify and better understand this potential effect.

4.3. Autoregressive model fits

Our multivariate autoregressive models for each subject and condition produced reliable and reasonable results (Lütkepohl, 2007b). The parameter to datapoint ratios were above 0.1, but averaging across subjects should have minimized any effects from overfitting. Also, multiple information criteria in Fig. S2 indicate that a model order of 32 was a reasonable choice. It should be noted that our model validation results indicate that the model is not as stationary and consistent as desired. This was unaffected when we tested higher model orders, but smaller window sizes might have improved this. We avoided window sizes below 400 ms because we wanted appropriate frequency resolution for our results and shorter time windows can degrade low-frequency connectivity results. While the models had lower consistency values than desired, all models were stable. Furthermore, the model-fitted cortical spectral density results (Figs. 4 and 5) closely match the cortical cluster ERSPs from previous studies (Peterson and Ferris, 2018a; Sipp et al., 2013; Varghese et al., 2014; Wagner et al., 2016). This gives us confidence that our model reasonably captured group-level activity.

4.4. Limitations and considerations

Our analysis was limited by the number of subjects and the potential for residual volume conduction effects on connectivity estimation. We used 29 subjects for our connectivity analysis and found a 2:1 ratio of subject number to average sample number per connection. While this on average gives us reasonable statistical power, we may have found more differences with a higher number of subjects. Also, it is possible that residual volume conduction is still affecting our connectivity results. We minimized this effect using independent component analysis, but volume conduction is still possible in source space (Brunner et al., 2016). We do not believe that volume conduction affected our results because we found specific perturbation-evoked connection patterns that sometimes differed from spectral power activity.

4.5. Conclusions

We used a multi-subject connectivity analysis to analyze source-localized information flow between cortical and muscular regions during sensorimotor perturbations. We found that physical pull perturbations to standing balance increased connectivity between the supplementary motor area and multiple motor areas, while visual rotation perturbations decreased connectivity between parietal and occipital areas These results may reflect cortical sensory integration performed to consistently maintain balance as sensorimotor input varied. Similar multi-subject connectivity analyses could potentially be used to assess both healthy and clinical populations, enhancing our understanding of cortical function during healthy balance and illuminating where the control problems lie when balance is impaired.

Funding

This research was sponsored by a Graduate Research Fellowship Program grant from the National Science Foundation (DGE 1256260). It was also sponsored by the Army Research Laboratory under Cooperative Agreement Number W911NF-10-2-0022 (Cognitive and Neuroergonomics Collaborative Technology Alliance) and the National Institutes of Health (R01 NS104772). The conclusions and views contained in this manuscript are those of the authors and should not be interpreted as representing the official policies, either expressed or implied, of the Army Research Laboratory or the United States Government.

Declarations of interest

None.

Acknowledgements

We would like to thank Estefania Rios for her assistance during data collections. We would also like to thank members of the Human Neuromechanics Laboratory for their input regarding data processing and analysis.

Appendix A. Supplementary data

Supplementary data to this article can be found online at https://doi.org/10.1016/j.neuroimage.2019.05.038.

References

Al-Subari, K., Al-Baddai, S., Tomé, A.M., Goldhacker, M., Faltermeier, R., Lang, E.W., 2015. EMDLAB: a toolbox for analysis of single-trial EEG dynamics using empirical mode decomposition. J. Neurosci. Methods 253, 193–205.

Artoni, F., Fanciullacci, C., Bertolucci, F., Panarese, A., Makeig, S., Micera, S., Chisari, C., 2017. Unidirectional brain to muscle connectivity reveals motor cortex control of leg muscles during stereotyped walking. Neuroimage 159, 403–416.

Astolfi, L., Cincotti, F., Mattia, D., Grazia Marciani, M., Baccala, L.A., de Vico Fallani, F., Salinari, S., Ursino, M., Zavaglia, M., Ding, L., Christopher Edgar, J., Miller, G.A., He, B., Babiloni, F., 2007. Comparison of different cortical connectivity estimators for high-resolution EEG recordings. Hum. Brain Mapp. 28, 143–157.

Benjamini, Y., Yekutieli, D., 2001. The control of the false discovery rate in multiple testing under dependency. Ann. Stat. 29, 1165–1188.

Blinowska, K.J., 2011. Review of the methods of determination of directed connectivity from multichannel data. Med. Biol. Eng. Comput. 49, 521–529.

Bolton, D.A.E., 2015. The role of the cerebral cortex in postural responses to externally induced perturbations. Neurosci. Biobehav. Rev. 57, 142–155.

Boonstra, T.W., Danna-Dos-Santos, A., Xie, H.-B., Roerdink, M., Stins, J.F., Breakspear, M., 2015. Muscle networks: connectivity analysis of EMG activity during postural control. Sci. Rep. 5, 17830.

Boonstra, T.W., Roerdink, M., Daffertshofer, A., van Vugt, B., van Werven, G., Beek, P.J., 2008. Low-alcohol doses reduce common 10- to 15-Hz input to bilateral leg muscles during quiet standing. J. Neurophysiol. 100, 2158–2164.

Brunner, C., Billinger, M., Seeber, M., Mullen, T.R., Makeig, S., 2016. Volume conduction influences scalp-based connectivity estimates. Front. Comput. Neurosci. 10, 121.

Caldwell, D.J., Wu, J., Casimo, K., Ojemann, J.G., Rao, R.P.N., 2017. Interactive web application for exploring matrices of neural connectivity. In: 2017 8th International IEEE/EMBS Conference on Neural Engineering (NER). https://doi.org/10.1109/ner.2017.8008287.

Carter, C.S., Braver, T.S., Barch, D.M., Botvinick, M.M., Noll, D., Cohen, J.D., 1998. Anterior cingulate cortex, error detection, and the online monitoring of performance. Science 280, 747–749.

Chang, C.-Y., Hsu, S.-H., Pion-Tonachini, L., Jung, T.-P., 2018. Evaluation of artifact subspace reconstruction for automatic EEG artifact removal. Conf. Proc. IEEE Eng. Med. Biol. Soc. 2018, 1242–1245.

Granger prediction. In: Cohen, M.X. (Ed.), 2014. Analyzing Neural Time Series Data: Theory and Practice. MIT Press.

Collings, R., Paton, J., Glasser, S., Marsden, J., 2015. The effect of vision impairment on dynamic balance. J. Foot Ankle Res. 8. https://doi.org/10.1186/1757-1146-8-s1-a6.

Delorme, A., Makeig, S., 2004. EEGLAB: an open source toolbox for analysis of single-trial EEG dynamics including independent component analysis. J. Neurosci. Methods 134, 9–21.

Delorme, A., Mullen, T., Kothe, C., Akalin Acar, Z., Bigdely-Shamlo, N., Vankov, A., Makeig, S., 2011. EEGLAB, SIFT, NFT, BCILAB, and ERICA: new tools for advanced EEG processing. Comput. Intell. Neurosci. 2011, 130714.

Ding, M., Bressler, S.L., Yang, W., Liang, H., 2000a. Short-window spectral analysis of cortical event-related potentials by adaptive multivariate autoregressive modeling: data preprocessing, model validation, and variability assessment. Biol. Cybern. 83, 35–45.

Ding, M., Bressler, S.L., Yang, W., Liang, H., 2000b. Short-window spectral analysis of cortical event-related potentials by adaptive multivariate autoregressive modeling: data preprocessing, model validation, and variability assessment. Biol. Cybern. 83, 35–45.

Domingo, A., Ferris, D.P., 2010. The effects of error augmentation on learning to walk on a narrow balance beam. Exp. Brain Res. 206, 359–370.

Domingo, A., Ferris, D.P., 2009. Effects of physical guidance on short-term learning of walking on a narrow beam. Gait Posture 30, 464–468.
Efron, B., Tibshirani, R.J., 1993. An Introduction to the Bootstrap.
Farina, D., Holobar, A., 2016. Characterization of human motor units from surface EMG decomposition. Proc. IEEE 104, 353–373.
Gramann, K., Ferris, D.P., Gwin, J., Makeig, S., 2014. Imaging natural cognition in action. Int. J. Psychophysiol. 91, 22–29.
Gramann, K., Gwin, J.T., Ferris, D.P., Oie, K., Jung, T.-P., Lin, C.-T., Liao, L.-D., Makeig, S., 2011. Cognition in action: imaging brain/body dynamics in mobile humans. Rev. Neurosci. 22, 593–608.
Granger, C.W.J., 1969. Investigating causal relations by econometric models and cross-spectral methods. Econometrica 37, 424.
Gu, Z., Gu, L., Eils, R., Schlesner, M., Brors, B., 2014. Circlize implements and enhances circular visualization in R. Bioinformatics. https://doi.org/10.1093/bioinformatics/btu393.
Gwin, J.T., Ferris, D.P., 2012. Beta- and gamma-range human lower limb corticomuscular coherence. Front. Hum. Neurosci. 6, 258.
Gwin, J.T., Gramann, K., Makeig, S., Ferris, D.P., 2011. Electrocortical activity is coupled to gait cycle phase during treadmill walking. Neuroimage 54, 1289–1296.
Gwin, J.T., Gramann, K., Makeig, S., Ferris, D.P., 2010. Removal of movement artifact from high-density EEG recorded during walking and running. J. Neurophysiol. 103, 3526–3534.
Hallett, M., 2008. The intrinsic and extrinsic aspects of freezing of gait. Mov. Disord. 23 (Suppl. 2), S439–S443.
Höller, Y., Uhl, A., Bathke, A., Thomschewski, A., Butz, K., Nardone, R., Fell, J., Trinka, E., 2017. Reliability of EEG measures of interaction: a paradigm shift is needed to fight the reproducibility crisis. Front. Hum. Neurosci. 11, 441.
Hotelling, H., 1936. Relations between two sets of variates. Biometrika 28, 321.
Huang, C.-Y., Lin, L.L., Hwang, I.-S., 2017. Age-related differences in reorganization of functional connectivity for a dual task with increasing postural destabilization. Front. Aging Neurosci. 9, 96.
Hwang, S., Agada, P., Kiemel, T., Jeka, J.J., 2014. Dynamic reweighting of three modalities for sensor fusion. PLoS One 9, e88132.
Jacobs, J.V., Horak, F.B., 2007. Cortical control of postural responses. J. Neural Transm. 114, 1339–1348.
Janssens, L., Brumagne, S., McConnell, A.K., Claeys, K., Pijnenburg, M., Burtin, C., Janssens, W., Decramer, M., Troosters, T., 2013. Proprioceptive changes impair balance control in individuals with chronic obstructive pulmonary disease. PLoS One 8, e57949.
Kamiński, M., Ding, M., Truccolo, W.A., Bressler, S.L., 2001. Evaluating causal relations in neural systems: granger causality, directed transfer function and statistical assessment of significance. Biol. Cybern. 85, 145–157.
Kline, J.E., Huang, H.J., Snyder, K.L., Ferris, D.P., 2016. Cortical spectral activity and connectivity during active and viewed arm and leg movement. Front. Neurosci. 10, 91.
Korzeniewska, A., Mańczak, M., Kamiński, M., Blinowska, K.J., Kasicki, S., 2003. Determination of information flow direction among brain structures by a modified directed transfer function (dDTF) method. J. Neurosci. Methods 125, 195–207.
Lau, T.M., Gwin, J.T., Ferris, D.P., 2014. Walking reduces sensorimotor network connectivity compared to standing. J. NeuroEng. Rehabil. 11, 14.
Liu, S., Guo, J., Meng, J., Wang, Z., Yao, Y., Yang, J., Qi, H., Ming, D., 2016. Abnormal EEG complexity and functional connectivity of brain in patients with acute thalamic ischemic stroke. Comput. Math. Methods Med. 2016, 2582478.
Lütkepohl, H., 2007b. New Introduction to Multiple Time Series Analysis. Springer Science & Business Media.
Macpherson, J.M., Horak, F.B., 2012. Posture. In: Kandel, E., Schwartz, J., Jessell, T., Siegelbaum, S., Hudspeth, A.J. (Eds.), Principles of Neural Science, fifth ed. McGraw Hill Professional, pp. 935–959.
Makeig, S., Bell, A.J., Jung, T.-P., Sejnowski, T.J., 1996. Independent component analysis of electroencephalographic data. Adv. Neural Inf. Process. Syst. 8, 145–151.
Marlin, A., Mochizuki, G., Staines, W.R., McIlroy, W.E., 2014. Localizing evoked cortical activity associated with balance reactions: does the anterior cingulate play a role? J. Neurophysiol. 111, 2634–2643.
Mierau, A., Pester, B., Hülsdünker, T., Schiecke, K., Strüder, H.K., Witte, H., 2017. Cortical correlates of human balance control. Brain Topogr. 30, 434–446.
Miller, K.J., Leuthardt, E.C., Schalk, G., Rao, R.P.N., Anderson, N.R., Moran, D.W., Miller, J.W., Ojemann, J.G., 2007. Spectral changes in cortical surface potentials during motor movement. J. Neurosci. 27, 2424–2432.
Mochizuki, G., Semmler, J.G., Ivanova, T.D., Garland, S.J., 2006. Low-frequency common modulation of soleus motor unit discharge is enhanced during postural control in humans. Exp. Brain Res. 175, 584–595.
Mullen, T., 2014. In: The Dynamic Brain: Modeling Neural Dynamics and Interactions from Human Electrophysiological Recordings (PhD). University of California, San Diego.
Mullen, T., Kothe, C., Chi, Y.M., Ojeda, A., Kerth, T., Makeig, S., Cauwenberghs, G., Jung, T.-P., 2013. Real-time modeling and 3D visualization of source dynamics and connectivity using wearable EEG. Conf. Proc. IEEE Eng. Med. Biol. Soc. 2013, 2184–2187.
Nuti, D., Masini, M., Mandalà, M., 2016. Benign paroxysmal positional vertigo and its variants. Handb. Clin. Neurol. 137, 241–256.
Oie, K.S., Kiemel, T., Jeka, J.J., 2002. Multisensory fusion: simultaneous re-weighting of vision and touch for the control of human posture. Brain Res. Cogn. Brain Res. 14, 164–176.
Palmer, J.A., Kreutz-Delgado, K., Makeig, S., 2006. Super-Gaussian Mixture Source Model for ICA. In: Lecture Notes in Computer Science, pp. 854–861.
Palmer, J.A., Makeig, S., Kreutz-Delgado, K., Rao, B.D., 2008. Newton method for the ICA mixture model. In: 2008 IEEE International Conference on Acoustics, Speech and Signal Processing. https://doi.org/10.1109/icassp.2008.4517982.
Petersen, T.H., Willerslev-Olsen, M., Conway, B.A., Nielsen, J.B., 2012. The motor cortex drives the muscles during walking in human subjects. J. Physiol. 590, 2443–2452.
Peterson, S.M., Ferris, D.P., 2018a. Differentiation in theta and beta electrocortical activity between visual and physical perturbations to walking and standing balance. eNeuro. https://doi.org/10.1523/ENEURO.0207-18.2018.
Peterson, S.M., Ferris, D.P., 2018b. Combined head phantom and neural mass model validation of effective connectivity measures. J. Neural Eng. https://doi.org/10.1088/1741-2552/aaf60e.
Peterson, S.M., Rios, E., Ferris, D.P., 2018. Transient visual perturbations boost short-term balance learning in virtual reality by modulating electrocortical activity. J. Neurophysiol. 120, 1998–2010.
Raez, M.B.I., Hussain, M.S., Mohd-Yasin, F., 2006. Techniques of EMG signal analysis: detection, processing, classification and applications. Biol. Proced. Online 8, 11–35.
R Core Team, 2017. R: A Language and Environment for Statistical Computing. R Foundation for Statistical Computing, Vienna, Austria.
Roeder, L., Boonstra, T.W., Smith, S.S., Kerr, G.K., 2018. Dynamics of corticospinal motor control during overground and treadmill walking in humans. J. Neurophysiol. https://doi.org/10.1152/jn.00613.2017.
Rowe, J., Stephan, K.E., Friston, K., Frackowiak, R., Lees, A., Passingham, R., 2002. Attention to action in Parkinson's disease: impaired effective connectivity among frontal cortical regions. Brain 125, 276–289.
Safieddine, D., Kachenoura, A., Albera, L., Birot, G., Karfoul, A., Pasnicu, A., Biraben, A., Wendling, F., Senhadji, L., Merlet, I., 2012. Removal of muscle artifact from EEG data: comparison between stochastic (ICA and CCA) and deterministic (EMD and wavelet-based) approaches. EURASIP J. Adv. Signal Process. 2012. https://doi.org/10.1186/1687-6180-2012-127.
Shine, J.M., Matar, E., Ward, P.B., Frank, M.J., Moustafa, A.A., Pearson, M., Naismith, S.L., Lewis, S.J.G., 2013. Freezing of gait in Parkinson's disease is associated with functional decoupling between the cognitive control network and the basal ganglia. Brain 136, 3671–3681.
Sipp, A.R., Gwin, J.T., Makeig, S., Ferris, D.P., 2013. Loss of balance during balance beam walking elicits a multifocal theta band electrocortical response. J. Neurophysiol. 110, 2050–2060.
Slobounov, S., Cao, C., Jaiswal, N., Newell, K.M., 2009. Neural basis of postural instability identified by VTC and EEG. Exp. Brain Res. 199, 1–16.
Snyder, K.L., Kline, J.E., Huang, H.J., Ferris, D.P., 2015. Independent component analysis of gait-related movement artifact recorded using EEG electrodes during treadmill walking. Front. Hum. Neurosci. 9. https://doi.org/10.3389/fnhum.2015.00639.
Solis-Escalante, T., van der Cruijsen, J., de Kam, D., van Kordelaar, J., Weerdesteyn, V., Schouten, A.C., 2018. Cortical dynamics during preparation and execution of reactive balance responses with distinct postural demands. Neuroimage 188, 557–571.
Theiler, J., Eubank, S., Longtin, A., Galdrikian, B., Doyne Farmer, J., 1992. Testing for nonlinearity in time series: the method of surrogate data. Physica D 58, 77–94.
Varghese, J.P., 2016. Cortical Activations Underlying Human Bipedal Balance Control (PhD). University of Waterloo.
Varghese, J.P., Marlin, A., Beyer, K.B., Staines, W.R., Mochizuki, G., McIlroy, W.E., 2014. Frequency characteristics of cortical activity associated with perturbations to upright stability. Neurosci. Lett. 578, 33–38.
Varghese, J.P., McIlroy, R.E., Barnett-Cowan, M., 2017. Perturbation-evoked potentials: significance and application in balance control research. Neurosci. Biobehav. Rev. 83, 267–280.
Wagner, J., Makeig, S., Gola, M., Neuper, C., Müller-Putz, G., 2016. Distinct β band oscillatory networks subserving motor and cognitive control during gait adaptation. J. Neurosci. 36, 2212–2226.
Wagner, J., Solis-Escalante, T., Grieshofer, P., Neuper, C., Müller-Putz, G., Scherer, R., 2012. Level of participation in robotic-assisted treadmill walking modulates midline sensorimotor EEG rhythms in able-bodied subjects. Neuroimage 63, 1203–1211.
Wagner, J., Solis-Escalante, T., Neuper, C., Scherer, R., Müller-Putz, G., 2013. Robot assisted walking affects the synchrony between premotor and somatosensory areas. Biomed. Tech. 58 (Suppl. 1). https://doi.org/10.1515/bmt-2013-4434.
Wagner, J., Solis-Escalante, T., Scherer, R., Neuper, C., Müller-Putz, G., 2014. It's how you get there: walking down a virtual alley activates premotor and parietal areas. Front. Hum. Neurosci. 8. https://doi.org/10.3389/fnhum.2014.00093.
Wu, Z., Huang, N.E., 2009. Ensemble empirical mode decomposition: a noise-assisted data analysis method. Adv. Adapt. Data Anal. 01, 1–41.